N O T I C E

THIS DOCUMENT HAS BEEN REPRODUCED FROM MICROFICHE. ALTHOUGH IT IS RECOGNIZED THAT CERTAIN PORTIONS ARE ILLEGIBLE, IT IS BEING RELEASED IN THE INTEREST OF MAKING AVAILABLE AS MUCH INFORMATION AS POSSIBLE

NASA CR-165361

CONTRACTOR REPORT

NAS3-22165

(NASA-CR-165361) STATIC TEST OF A FAN-POWERED CHIN NOZZLE FOR V/STOL APPLICATIONS Final Report (Boeing Military Airplane Development) 37 p HC A03/MF A01 CSCL 01A G3/02

N81-29093

Unclas 27101

STATIC TEST OF A FAN-POWERED "CHIN" NOZZLE FOR VISTOL APPLICATIONS

Victor Salemann

Boeing Military Airplane Company

AUG 1981
RECEIVED
NASA STI FACILITY
ACCESS DEPT.

Prepared for

National Aeronautics and Space Administration

NASA Lewis Research Center
Contract NAS 3-22165

TABLE OF CONTENTS

LIST OF FIGURES

STATIC TEST OF A FAN-POWERED "CHIN" NOZZLE FOR V/STOL APPLICATIONS

SUMMARY

The chin-nozzle concept for thrust vectoring was developed by Boeing-Vertol for the Navy Type A V/STOL aircraft. In hover, part of the fan flow is exhausted downward immediately behind the fan, while the rest of the engine airflow is deflected by a blown flap system. This results in a four-poster VTOL configuration with only two fans and a crosshaft, and in an aircraft with excellent STOL capabiities. The scope of this program was to design and build a model of the chin nozzle to be tested by NASA-Lewis behind a 12" tip-turbine powered fan and to provide data analysis. The initial objective was to obtain measurements of fan exit pressure distribution, fan blade stresses, and performance of the chin nozzle as a function of proximity of the chin nozzle to the fan. However, previous NASA tests showed that the 12" tip-turbine driven fan, because of its structural design, did not provide suitable blade stress information. As a result, this test objective was deleted.

The model consisted of a cowl and chin nozzle cascade, three aft nozzles and sets of cascade blockers to permit variation of chin/aft nozzle flow split from 25/75% to 75/25%, the range needed for control of the aircraft. Two spacers to be inserted between the fan and chin nozzle were also built.

Testing included measurement of thrust split, fan total pressure profiles, internal wall statics and flow visualization. Flow split could not be determined due to instrumentation limitations.

Fan exit pressure distortion caused by the cowl shape approaching the chin nozzle caused a drop in fan discharge pressure near the blade tip in the quadrant nearest the chin nozzle. The distortion was primarily a result of cowl curvature and was not significantly affected by changes in flow split. Spacers inserted between the fan and chin nozzle reduced the exit pressure distortion.

Thrust split achieved was close to design values up to a 50/50 split. For design chin nozzle thrust of 71 and 75%, the measured values were 55 and 65%. Flow visualization showed that the cascade had large areas of separation on the pressure side. This is thought to be caused by internal flow turning approaching the cascade resulting in excessive negative angles-of-attack at the vane leading edge, particularly near the aft end of the cascade.

Cascade thrust efficiency is probably adversely affected by the flow separation at the highest cascade open area setting. It appears necessary to tailor the cascade vane camber to the location of each vane, with the aft vanes having opposite camber to be aligned with the oncoming flow. Further work to determine flow split and improve cascade design and performance is recommended.

INTRODUCTION

The chin nozzle test program is an outgrowth of the Navy Type A V/STOL Program of 1977. Several concepts such as tilt nacelles, thrust vectoring and thrust augmentation with vectoring were submitted to the Navy. NASA supported this program by tests in key propulsive areas such as tilt inlets, thrust deflection concepts and complete configuration tests.

The chin nozzle concept was proposed by Boeing-Vertol. The aircraft, propulsion system and nacelle are shown on Fig. 1. This concept provides a 4-Poster VTOL aircraft with a minimum of shafting, gearboxes and fans. Each fan is driven by two side-by-side turboshaft engines through a gearbox. Since the aft stream is turned by a flap system, the aircraft also exhibits lift augmentation in STOL, providing excellent STOL overload capability.

A large moment arm between the front and rear "posts" is desirable to minimize variations in thrust split required for control. On the other hand, a short nacelle is desirable to keep down weight and provide side visibility for the pilot. Therefore, it is desirable to deflect the portion of the flow destined for the "chin" nozzle as close to the fan exit plane as practical. A primary concern was that this diversion would produce a large fan exit pressure distortion which may adversely affect fan stall margin and fan performance. Data on chin nozzle performance and design information were also desired.

Existing applications did not provide sufficient information for chin nozzle design. Fan cascade thrust reversers on high bypass ratio engines are nearly symmetrical, the turning angle is much higher and efficiency requirement not as stringent. Data from the "Deflector/Nozzle" Program, Ref. 1, provides distortion data in narrow, annular flow passages due to single or twin nozzles in the duct wall typical of fan ducts in low bypass ratio fan engines.

A simplified 2-D potential flow analysis of the internal flow for 30° of turning is shown on Fig. 2. This value was selected as representative of internal turning required approaching the cascade. The distortion in the fan exit plane appeared minimal, less than caused by bifurcations in commercial airplane nacelles. Real flow with actual goemetry, including a centerbody due to the gearbox and core engines, could produce more severe distortion.

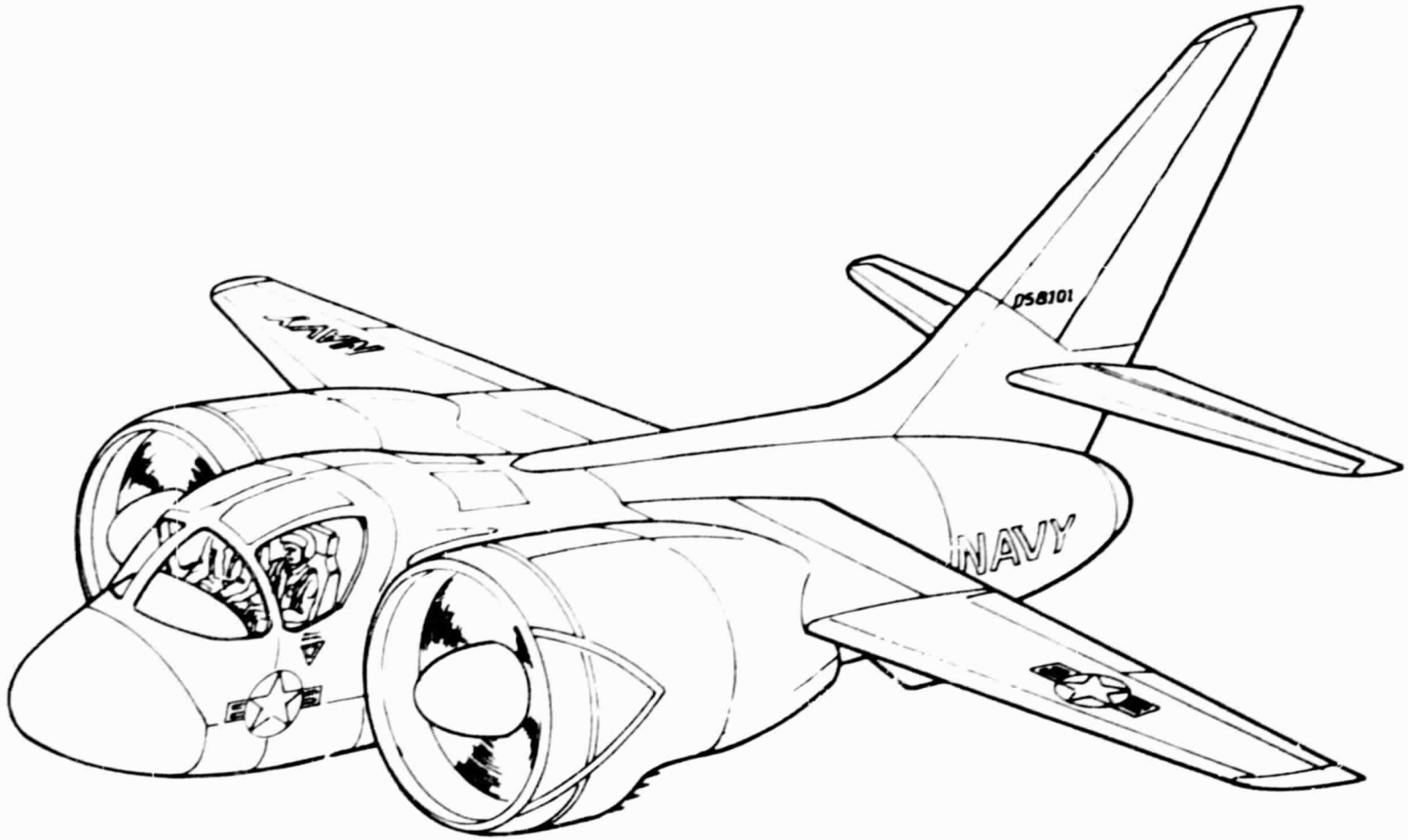

Figure 1. Blown Flap V/STOL A Airplane Concept

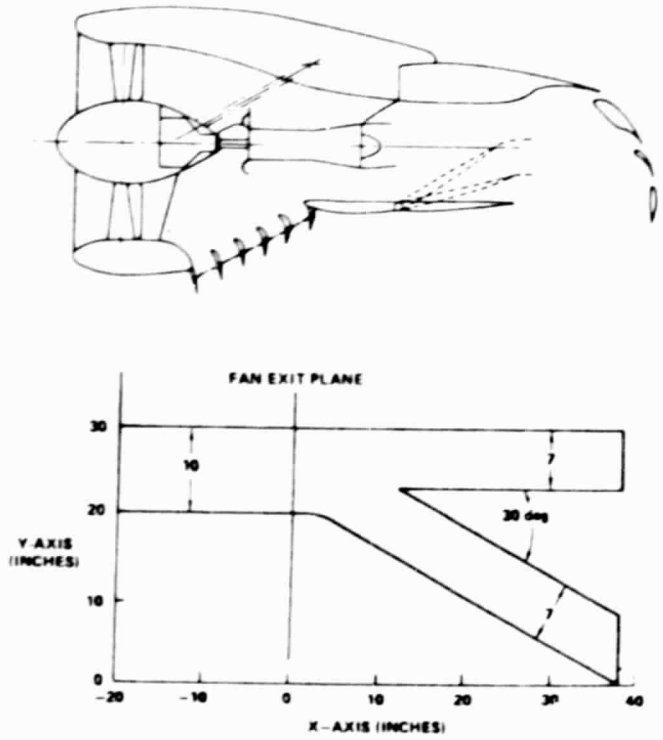

Equivalent Duct

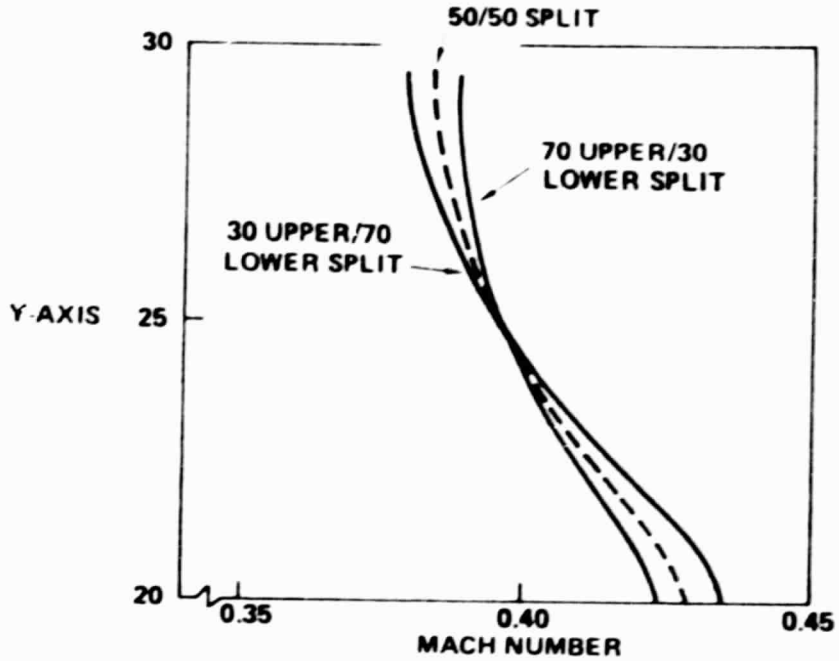

Figure 2. Mach Number Distribution Across Equivalent Duct in the Fan Exit Plane

SYMBOLS AND ABBREVIATIONS

A_{AFT}	Aft nozzle exit area
A_{CHIN}	Chin nozzle net exit area
A_{TOT}	$A_{AFT} + A_{CHIN}$
C_{DAFT}	Aft nozzle flow coefficient
C_{DCHIN}	Chin nozzle flow coefficient
C_{VERT}	See Pg. 8
C_{VCOMP}	See Pg. 18
F_{AFT}	Aft nozzle thrust
F_{AXIAL}	Axial force
F_{NORMAL}	Normal force
FPR	Fan probe total/ambient static pressure
g	Gravitational constant
M	Mach number
PHI, ϕ	Peripheral angle
P_s	Local static pressure
P_{T2}	Average fan discharge total pressure
R/H	Radius to probe/annulus height
V_{IDEAL}	Ideal fully expanded velocity
W_{FAN}	Fan weight flow

PROGRAM SCOPE AND OBJECTIVES

Since available data were so limited, a test program was initiated to measure exit pressure distortion effects on the fan due to a chin nozzle over a range of flow split and fan-to-nozzle spacing. The initial scope of the program was to design and build a model for a 12" tip-turbine driven fan, observe testing by NASA and analyze and report the results. The model and variable components are shown on Fig. 3. Measurements were to include fan inlet flow, turbine flow and aft nozzle flow survey, fan exit total pressure

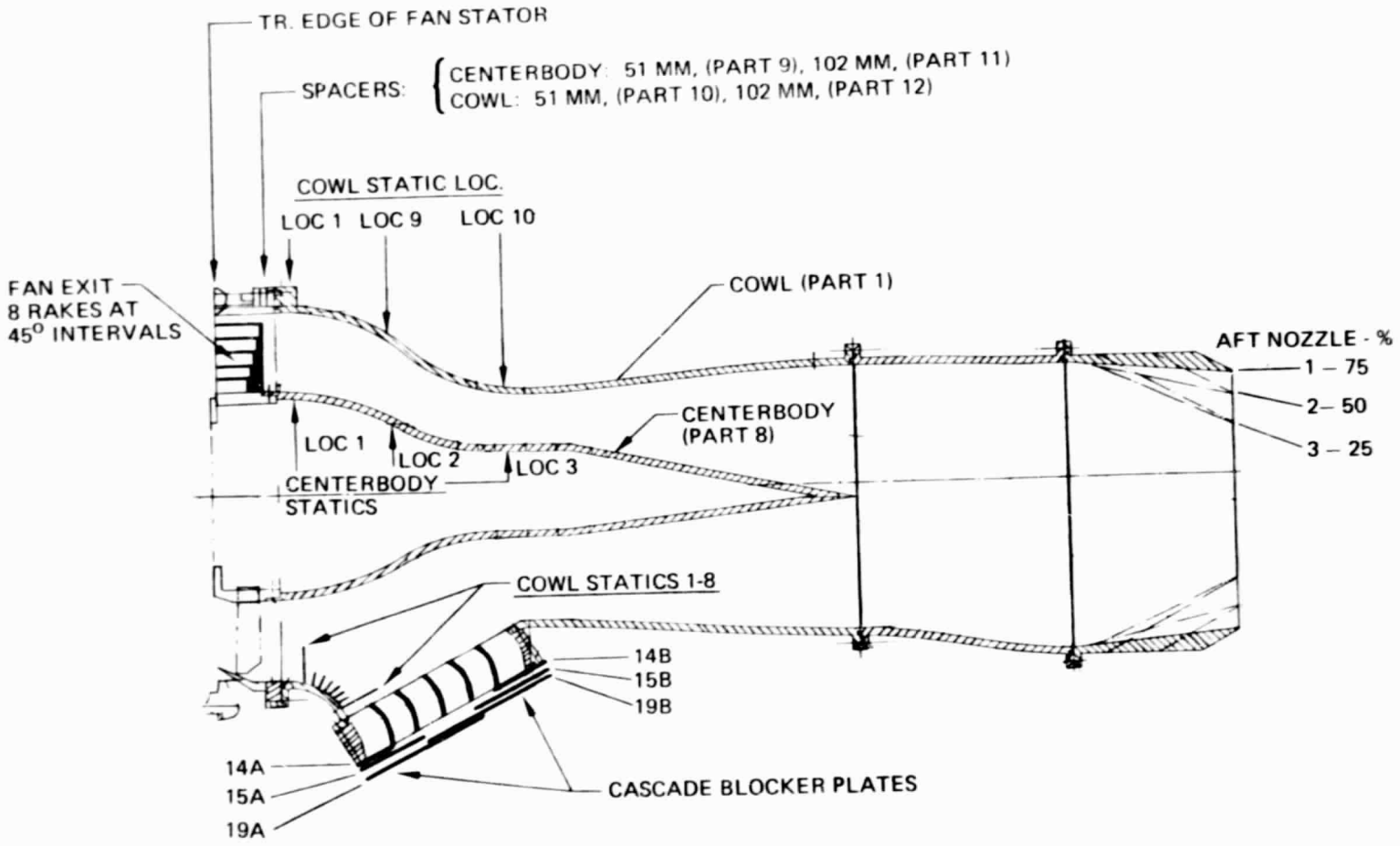

Figure 3. Chin Nozzle Model

distribution, cowl centerbody static pressure distributions and force data. Initial objectives included measurement of fan blade stresses, but was deleted due to the structural design of the shrouded fan which did not provide suitable blade stress information. Aft nozzle exit surveys using existing, fixed rakes were attempted but were felt to be too coarse for the distortion encountered, resulting in unreasonable indicated flow split between the chin nozzle and aft nozzle. More detailed exit flow surveys are planned using a translating rake. During the testing it became evident that the actual thrust split was well below theoretical for the highest thrust split of approximately 70% to the chin nozzle. Flow visualization studies were conducted to gain a better understanding for the design and operating modes of a chin nozzle.

MODEL DESIGN

The model was designed to fit the NASA-supplied 12" tip-turbine powered fan hardware. The centerbody representing the gearbox and core engines was waisted in the region of the core engine inlets to allow better downflow towards the chin nozzle. The cowl was offset in a downward direction relative to the centerbody to minimize changes in fan discharge back pressure as a function of chin nozzle area by forcing the flow to cross to the underside of the centerbody even when the aft nozzle area is large.

The plane of the chin nozzle cascade was set at 30^{o} to the horizontal and the discharge angle of the cascade at 75^{o}. This discharge angle would result in a purely vertical lift force on the aircraft when the aircraft angle-of-attack is 15^{o}, which was a normal landing attitude but could also be easily achieved for liftoff by a temporary thrust transfer to the chin nozzles.

Reducing the nominal jet turning angle for hovering in this manner pays off in improving the thrust efficiency, particularly that of the aft nozzle/flap combination, see Fig. 2. Turning by slotted flaps depends partly on the coanda effect, whose effectiveness starts to decrease at about 60^{o} of turning. Reducing the operating range of the chin nozzle discharge angle also reduces the maximum chin nozzle cascade area requirement with benefits in nacelle weight and drag.

The range of front/aft flow split was derived from aircraft control studies, resulting in a nominal requirement from 30/70 to 70/30. The cascade was sized to this requirement assuming a 90% flow coefficient. This flow range was achieved by building three aft nozzles and blocking part of the cascade area as shown on Fig. 3. The fan had not been calibrated at the time the model was built, so the aft nozzles were undersized 20% as a precautionary measure. Being conical nozzles, they could be easily opened up by shortening them to match the fan nozzle area requirements.

Cascade flow area would be controlled on the airplane by selectively shutting off some passages. The passages could be blocked in a symmetrical manner or working from either end. Blockers to simulate all three modes were manufactured.

Should the fan exit pressure distortion prove excessive at the fan-to-chin nozzle spacing selected, 51mm (2 inch) and 102mm (4 inch) spacers were built to allow increasing the distance to the chin nozzle.

Internal pressure instrumentation is shown on Fig. 3 and included static taps on the cowl and centerbody, the NASA-suppled fan exit rake, and external survey rakes for the aft nozzle.

The model cowl was designed with a flanged joint ahead of the aft nozzle to permit installation of a screen, if required, to smooth out the aft nozzle flow to improve survey accuracy.

TEST APPARATUS

The model was tested at NASA-Lewis on the vertical thrust stand. The test setup is shown on Fig. 4 and 5. Turbine air is metered before delivery to the model. Fan air is metered by the inlet bellmouth. Turbine discharge air is collected and exhausted on opposite sides, normal to the thrust and lift direction. The model is supported by a 6-component balance. Pressures were measured on scanivalves mounted external to the model. A color television monitor was used to observe the model and flow visualization patterns. Data were recorded and reduced to engineering units. Complete printouts and selected data on tape were supplied for data analysis. Flow visualization results were recorded on videotape and still color photographs.

RESULTS

Performance of the chin nozzle was evaluated by comparing the measured "vertical thrust coefficient," C_{VERT}, to the design value. C_{VERT} is defined as the ratio of the measured normal force to the ideal thrust based on the total fan flow. The design value is based on the above ideal thrust, the chin nozzle goemetric area, estimated flow coefficient and discharge direction.

$$C_{VERT} = \frac{g \; F_{NORMAL}}{W_{FAN} \; V_{IDEAL}}$$

$$C_{VERT,\,DESIGN} = \frac{W_{FAN} \; V_{IDEAL} \quad \times g \times \%\ \text{SPLIT} \times \cos 75^{o}}{g \times W_{FAN} \; V_{IDEAL}}$$

The test parameter "% split" is derived from the areas and estimated flow coefficients of the chin and aft nozzles. It also represents the design thrust split if both nozzles have similar velocity coefficients

$$\%\ \text{SPLIT} = \frac{A_{CHIN} \, C_{D_{CHIN}} \quad \times 100}{A_{CHIN} C_{D_{CHIN}} + A_{AFT} C_{D_{AFT}}}$$

Data were obtained over a range of fan speeds from 60% to 90%. Fan pressure ratio vs. fan speed for three sets of chin and aft nozzles is shown on Fig. 6. The total exit area of each chin nozle and aft nozzle set was held approximately constant. Therefore, the total fan flow and average fan exit conditions are the same for all nozzle sets at equal fan total pressure ratios. The nominal fan pressure ratio of the blown flap V/STOL A airplane was 1.22, corresponding to 75% RPM.

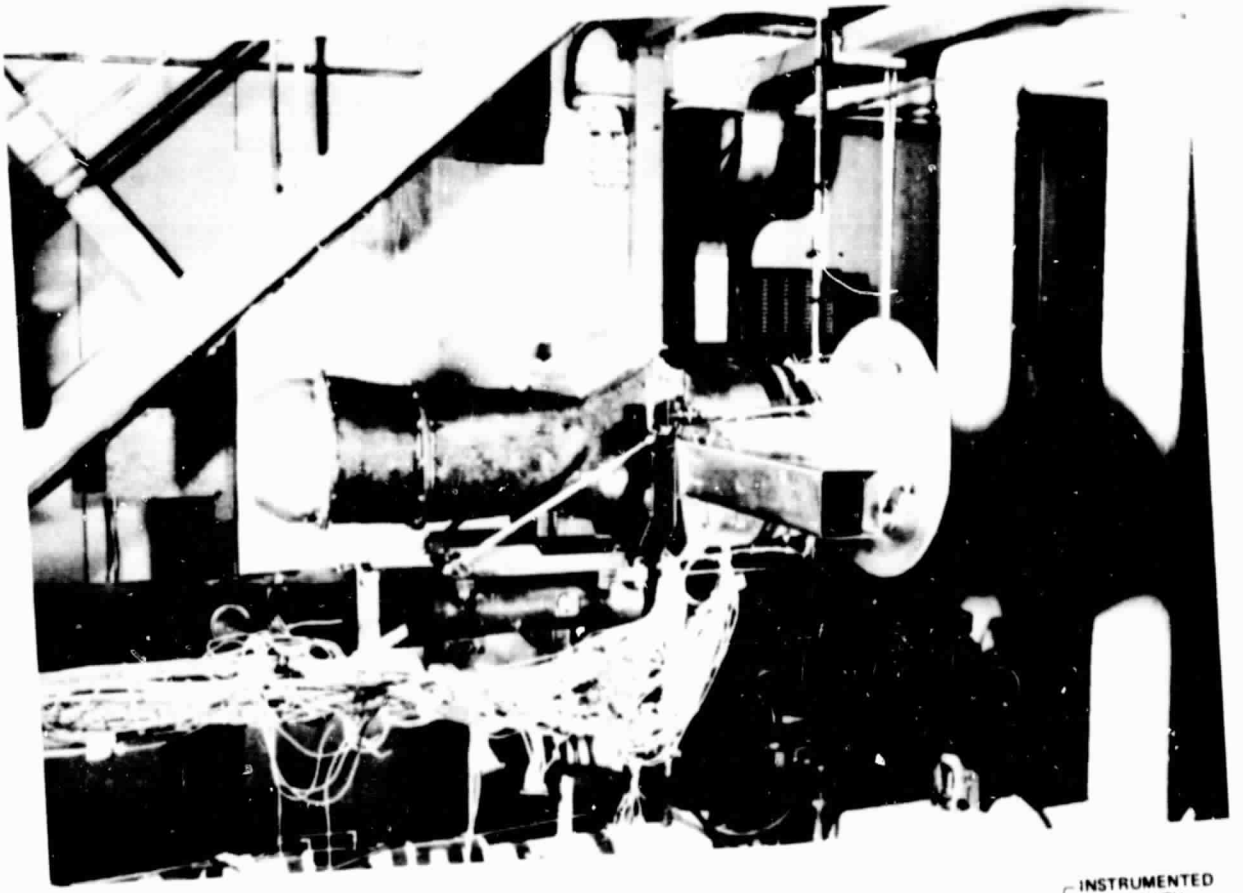

Figure 4. Test Setup

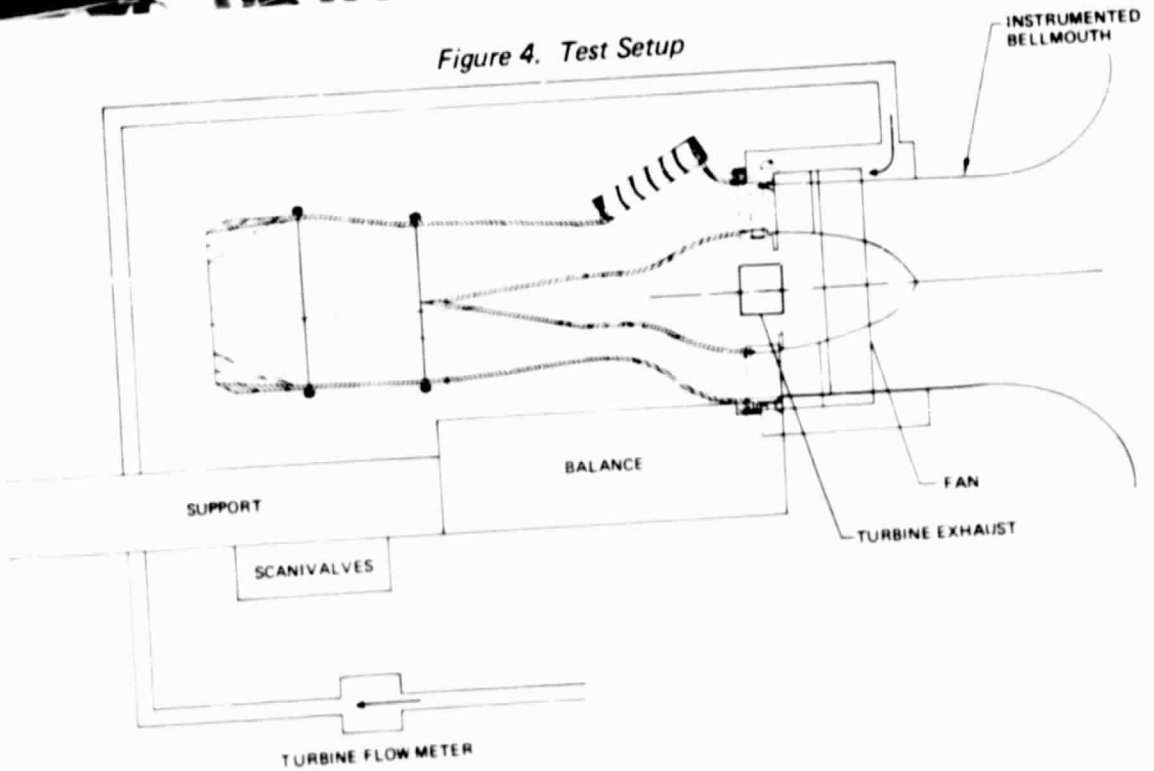

Figure 5. Schematic of Test Setup

ORIGINAL PAGE IS
OF POOR QUALITY

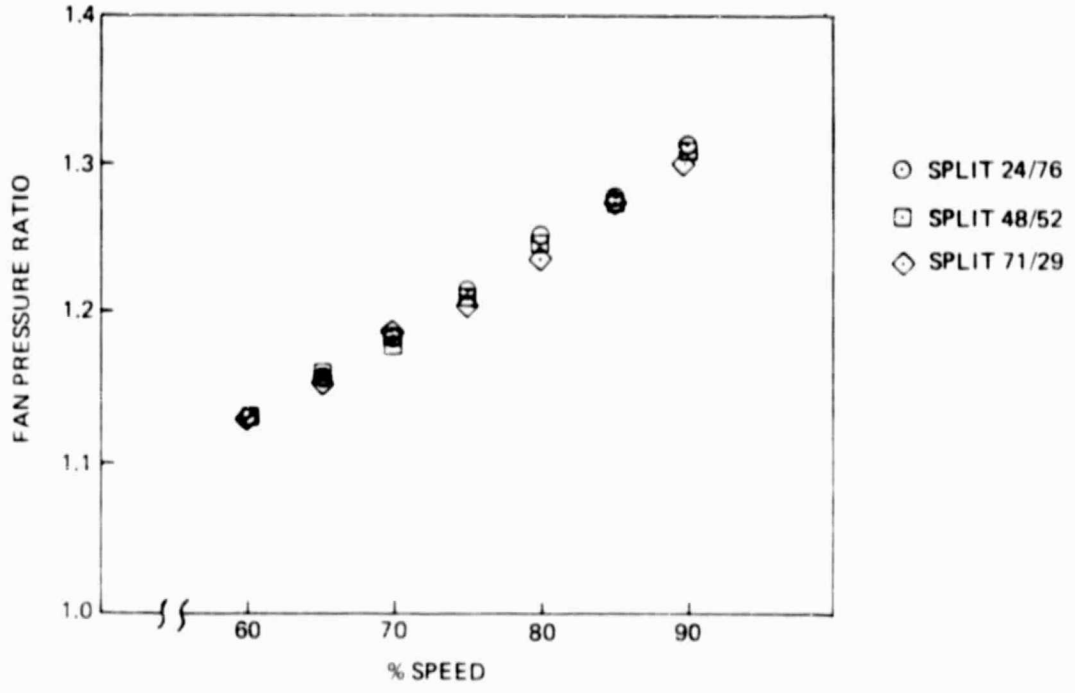

Figure 6. Fan Operating Line

Aft nozzles were intentionally built 20% undersize to facilitate matching the total effective area of each set to fan requirements. Test results indicated that the nominal areas selected were correct. The aft nozzles were enlarged and most test conditions except tests with the longest spacing (153 MM) were repeated. Figure 7 shows results with both sets of aft nozzles. The difference between measured and design C_{VERT} is a measure of deficiency in the nozzle. Results show that the chin nozzle thrust performance decreases with increased chin nozzle area. This may be caused by a decreasing discharge coefficient, decreasing thrust vector angle or fanning-out of the chin nozzle flow, or decreasing velocity coefficient. Actual C_{VERT} was somewhat closer to the design value with the initial aft nozzle size which was smaller.

Flow visualization was employed to attempt to find the reason for the low thrust output of the chin nozzle. Dabs of artist's oil colors were arranged in rows of different colors on the cascade vanes, cowl, centerbody and splitter plates mounted in the exhaust flow, as shown in Fig. 8. Flow at the desired fan pressure ratio was established and held for 10-15 seconds until the pattern, as seen on the television monitor, was established. The model was shut down, examined and photographed. Results are shown on Figs. 9 to 13 for the case of maximum chin nozzle open area. Fig. 9 shows the suction and pressure side of the chin nozzle cascade. Separation and backflow are indicated on the pressure side of the last two (aft) vanes of the cascade by lack of development of a flow pattern or even backward flow. (A pattern of dots where each row is a different color is particularly helpful to establish direction of flow.) The flow pattern on the cowl also indicated that the flow approached the aft end of the cascade from the rear, resulting in an excessively high negative angle-of-attack and separation. This is illustrated on Fig. 10. Flow patterns on the centerbody, Fig. 11, indicated twin stagnation points and vortices on the side facing the chin nozzle, as might be expected. The pattern on the sides, Fig. 11, shows a cross flow in the area where the core engine inlet would be, giving rise to concern for the stability of core engines. Losses due to flow across the centerbody probably contributed to the lower performance of the chin nozzle at higher flow rates. Splitter plates mounted in the chin nozzle exit flow show the flow direction and intensity. The plates were mounted in the middle of the right and left half of the chin nozzle. The flow patterns shown in Fig. 12 are not symmetrical and show some low-velocity regions, but the exhaust vector angle is close to design.

The effect of distance from the fan to the cascade on C_{VERT} is shown on Fig. 13. The difference between design and actual C_{VERT} decreases with increased spacing at the highest thrust split.

Since it appeared that the aft vanes were not properly cambered for the local flow direction, tests were run with the aft vane removed and all vanes removed. Results in terms of C_{VERT} were disappointing, as shown on Fig. 14. Removal of one vane resulted in no change in C_{VERT}, while removal of all vanes reduced it further. Oil flow and tuft flow visualization indicated that the exit flow was approximately perpendicular to the cascade plane when all vanes were removed. The exit angle was therefore approximately 60° without vanes compared to 75° with vanes. The reduced angle would result in approximately 10% lower vertical thrust component, which is slightly more than the measured reduction.

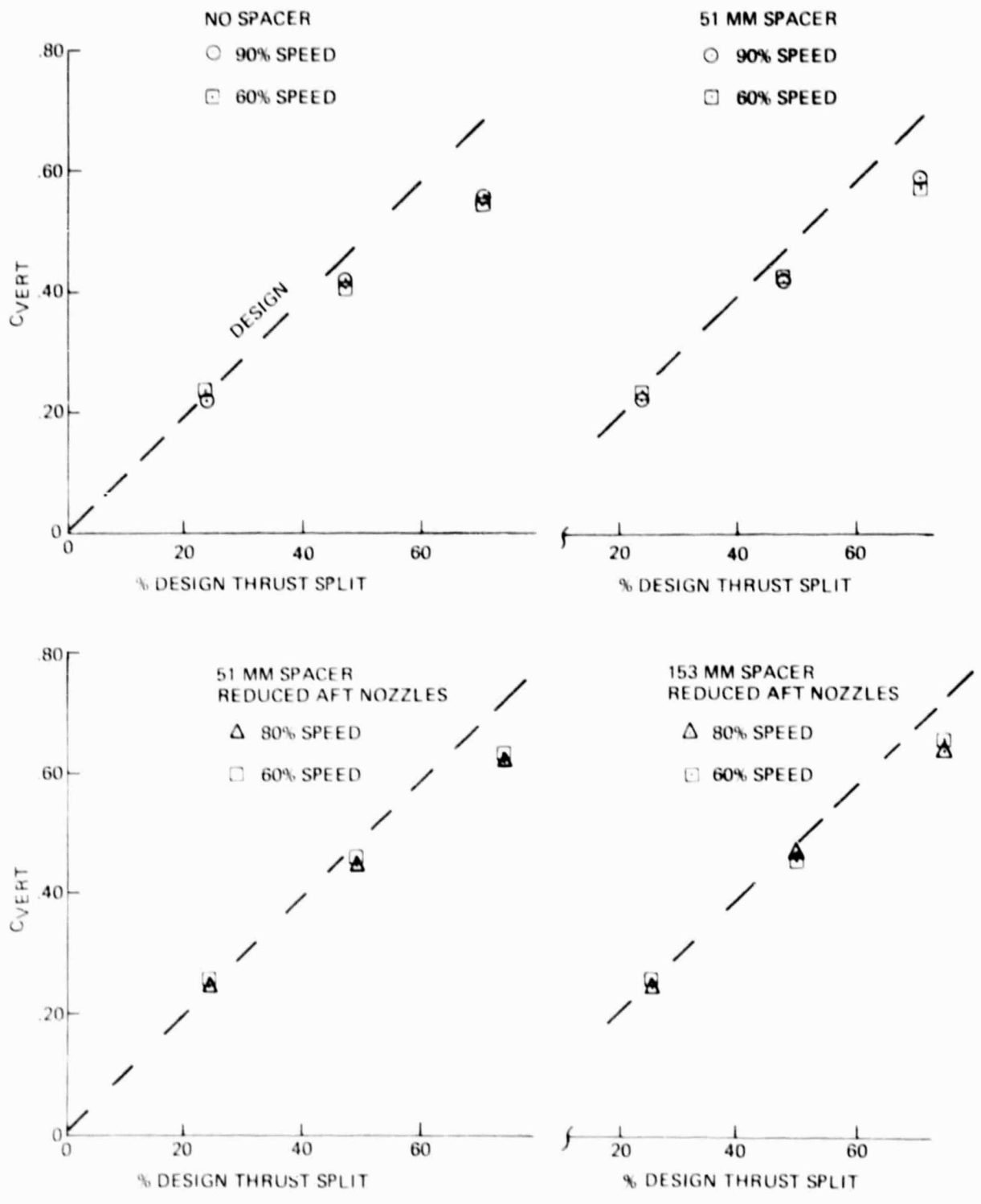

Figure 7. Effect of Chin Nozzle to Fan Spacing on Vertical Thrust Component

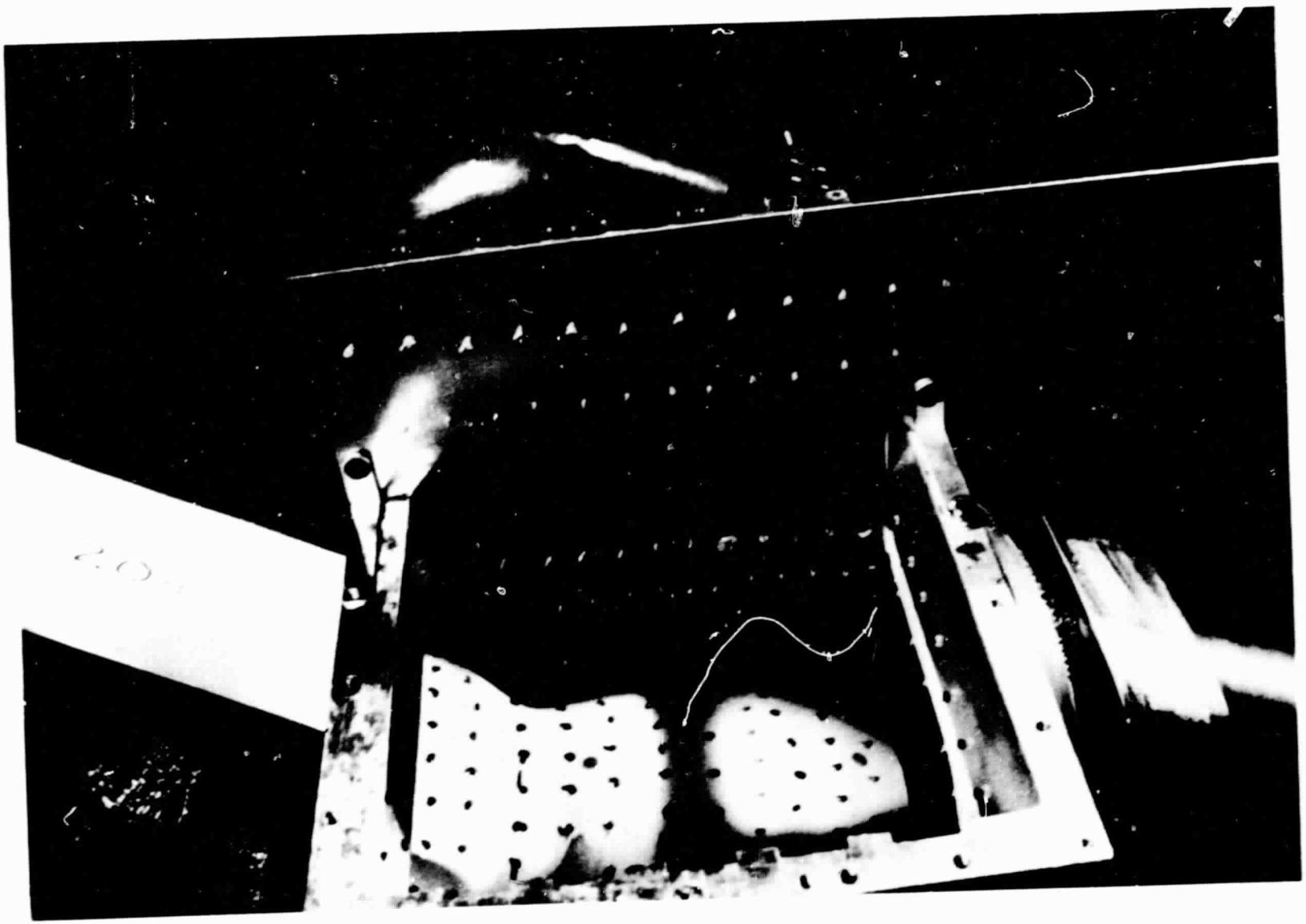

Figure 8. Flow Visualization Dot Pattern

PRESSURE SIDE
FORWARD END

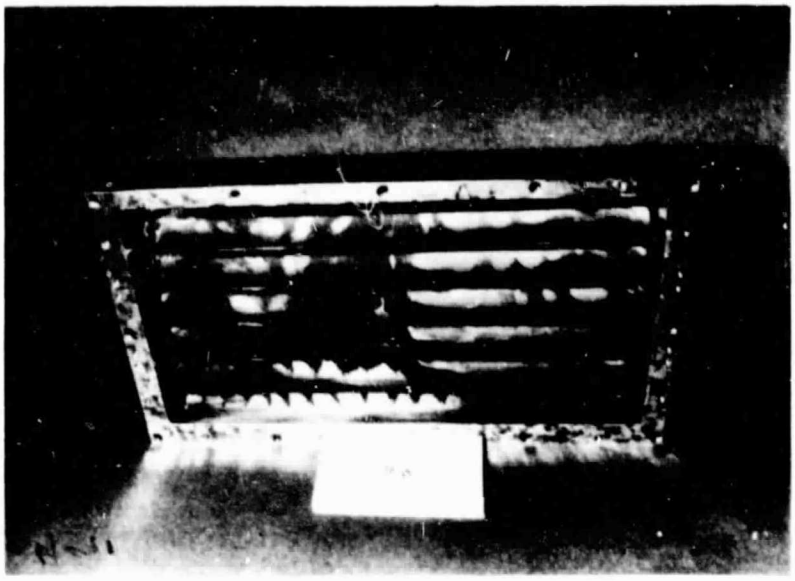

AFT END

LOOKING UPSTREAM

SUCTION SIDE
AFT END

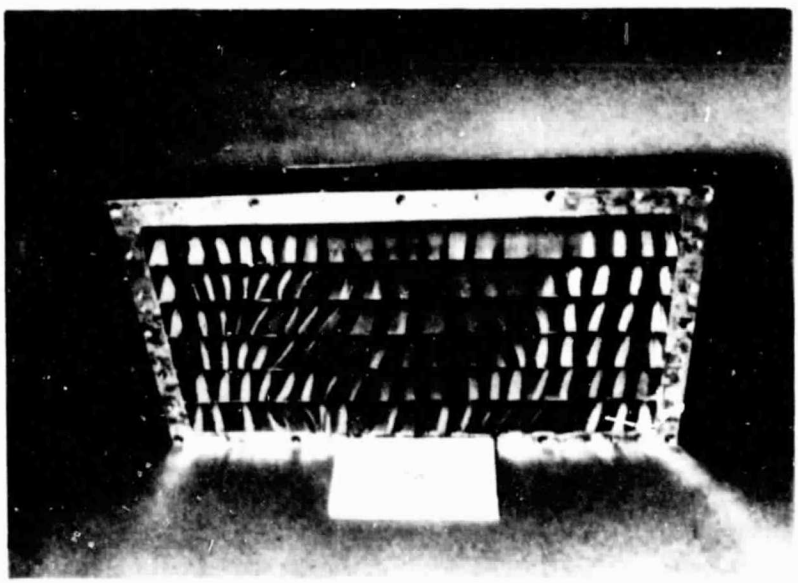

FORWARD END

Figure 9. Flow Visualization on Cascade

ORIGINAL PAGE IS
OF POOR QUALITY

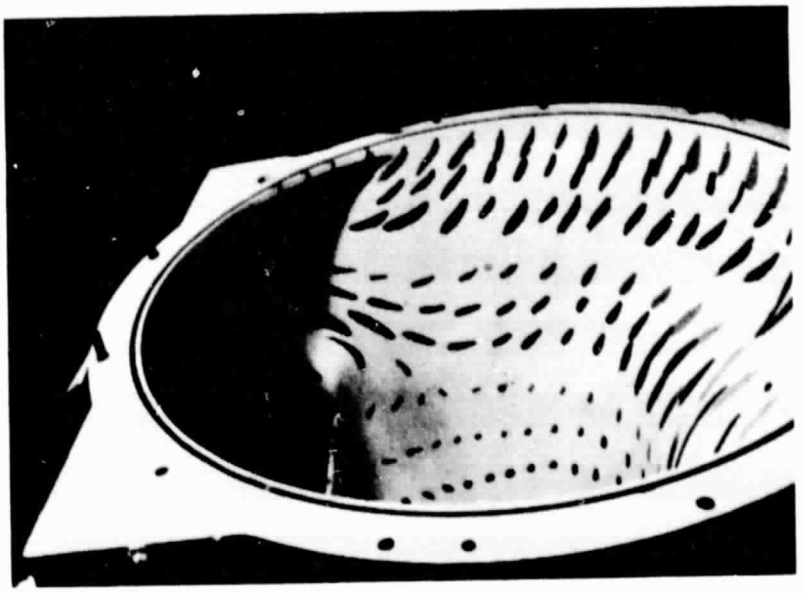

Figure 10. Flow Visualization on Cowl

Figure 11. Flow Visualization on Centerbody

ORIGINAL PAGE IS
OF POOR QUALITY

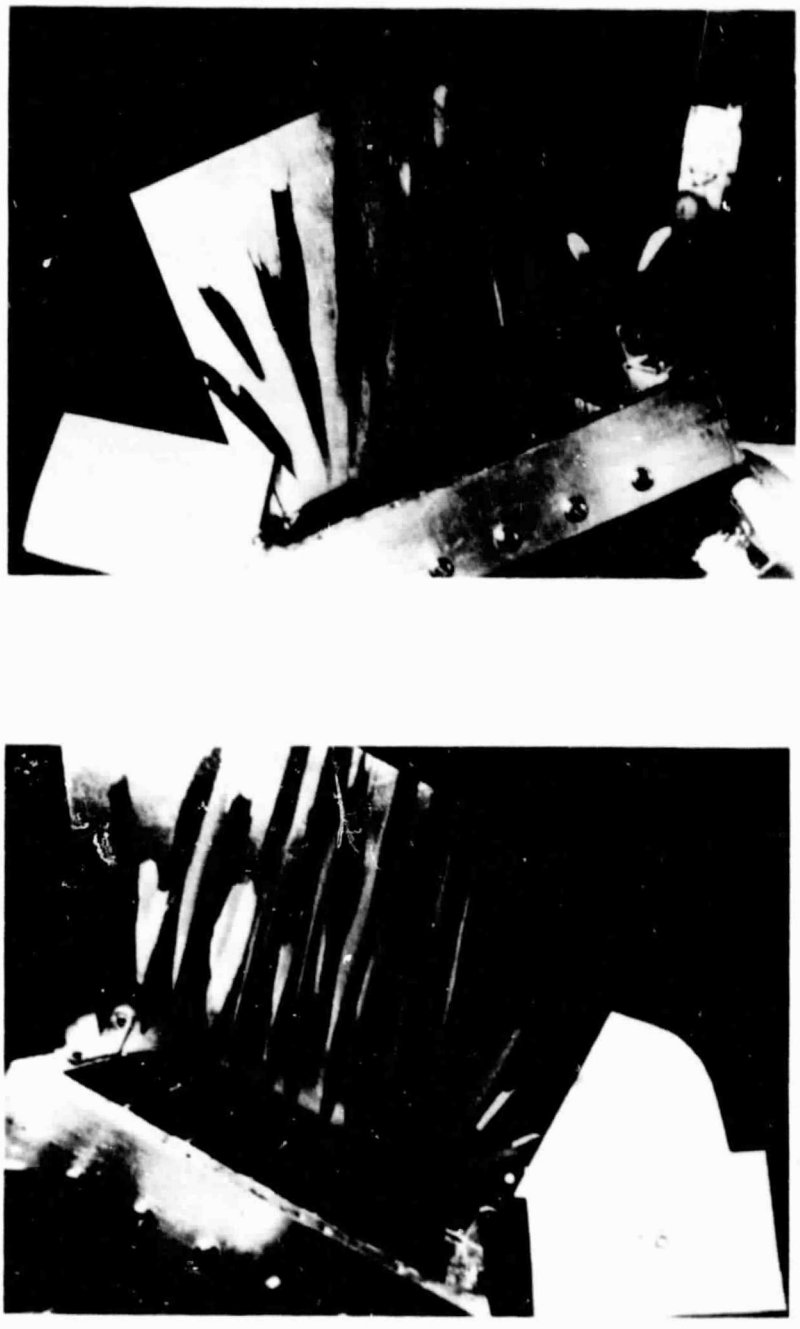

Figure 12. Jet Flow Visualization on Splitter Plates

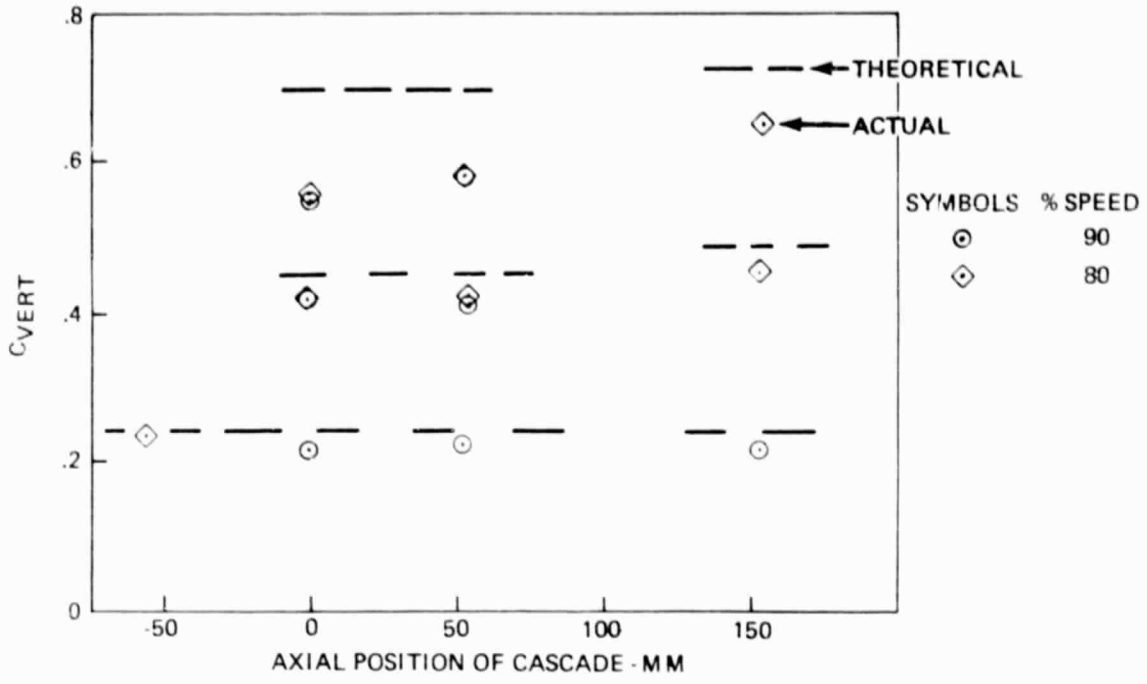

Figure 13. Effect of Cascade Location on Vertical Thrust Coefficient

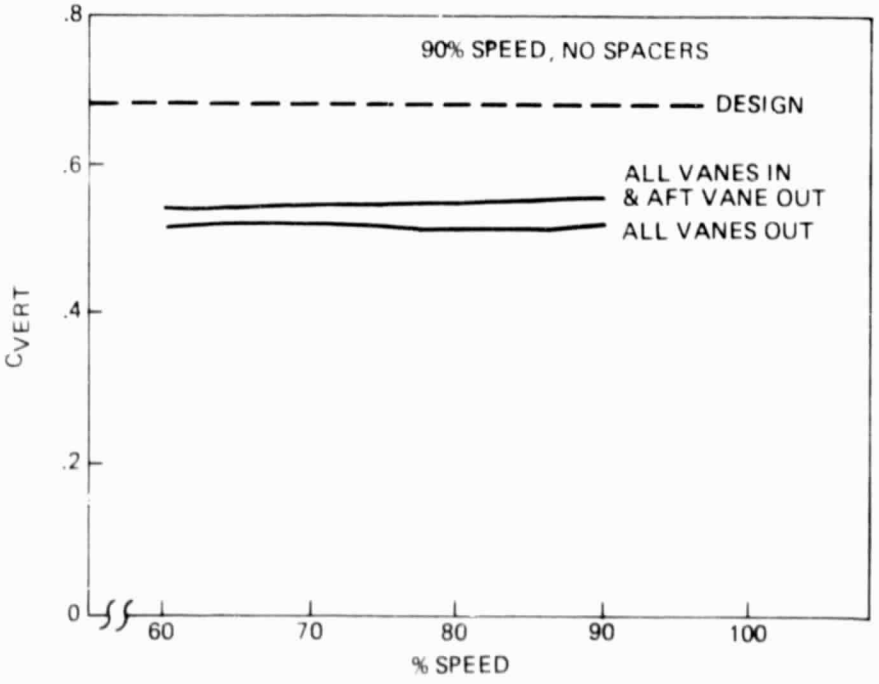

Figure 14. Effect of Vane Removal on Vertical Thrust Coefficient

Breakdown of the difference between measured and "design" $C_{V_{VERT}}$ into components requires additional data such as actual flow through each nozzle and average total pressure delivered by the fan to each nozzle or thrust direction of each nozzle. The latter is known approximately for the chin nozzle based on oil flows and for the aft nozzle based on geometry. If the aft nozzle thrust is assumed to be axial, and the chin nozzle thrust at 75 degrees to the horizontal as designed, the thrust of each nozzle can be obtained from the force data as follows:

$$F_{CHIN} = \frac{F_{NORMAL}}{\sin 75^o}$$

$$F_{AFT} = F_{AXIAL} - \frac{F_{NORMAL}}{\sin 75^o} \times \cos 75^o$$

The composite thrust efficiency of both nozzles can be obtained by dividing the algebraic sum of their thrusts by the ideal thrust based on total airflow, average nozzle pressure ratio and average temperature:

$$C_{V_{COMP}} = \frac{F_{CHIN} + F_{AFT}}{\frac{W_{FAN}}{g} V_{IDEAL,\ FAN}}$$

The result is equivalent to the case where both nozzles discharge in the same direction but with different efficiencies, such as in short duct fan engines.

Since the aft nozzles are conical with good approach conditions from the charging station, which is the fan exit rake, their efficiency is expected to be high, and therefore, a low value of $C_{V_{COMP}}$ would be ascribed to the chin nozzle.

The composite C_V is plotted against percent design thrust split on Fig. 15. It is seen that the C_V is .97 to .99 when most of the thrust is produced by the aft nozzle and deteriorates to .88 to .91 when the thrust split switches in favor of the chin nozzle.

As the thrust split is increased in favor of the chin nozzle, the aft nozzle area decreases and duct Mach number also decreases aft duct losses. In addition, fan exit rake profiles showed a high pressure ration at 0^o, opposite to the angular location of the cascade. Also, if it is assumed that the diversion of the flow from the fan to the chin nozzle is symmetrical, the average total pressure of the aft nozzle flow would increase as chin nozzle flow increases, because the rake at 0^o consistently registered a higher total pressure than average. That flow would always be expected to exit through the aft nozzle, but, when the aft nozzle is small, there would be less flow originating from neighboring segments of the fan present to dilute the effect of the higher-pressure segment. So, since the ideal thrust per unit airflow probably increases, and since the duct losses probably decrease, it would be reasonable to expect that the aft nozzle thrust contribution per unit airflow is probably increasing as aft nozzle size is decreased. Therefore,

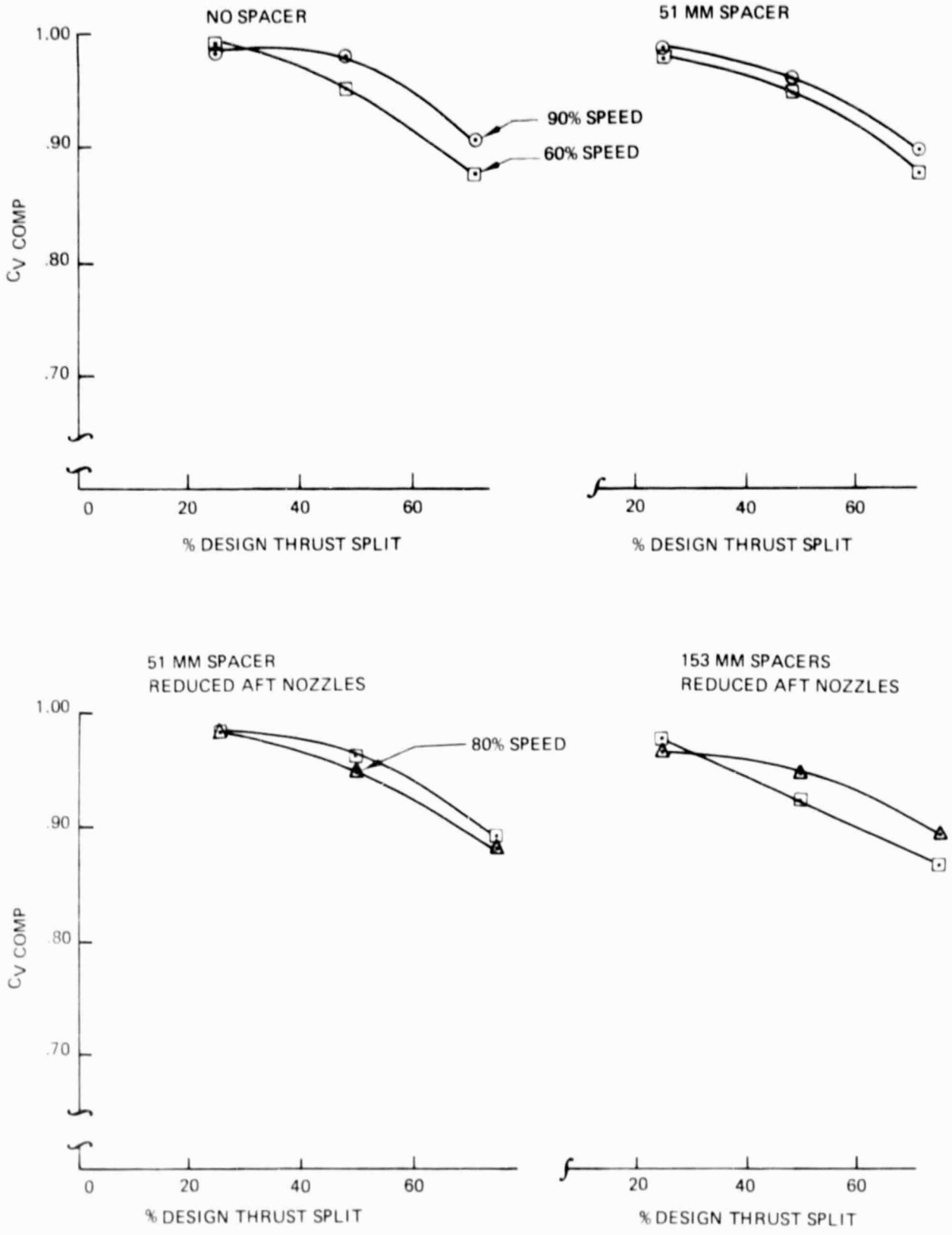

Figure 15. Effect of Chin Nozzle to Fan Spacing on Composite Velocity Coefficient

any drop in composite C_V is attributed to the chin nozzle and to duct losses to the chin nozzle. The increase in the chin nozzle losses between 24/76 split and 71/29 split is somewhat greater than indicated by the change in composite C_V, because 29% of the thrust is still generated by the more efficient aft nozzle in the 71/29 case. Therefore, the chin nozzle thrust loss is approximately 30% greater than indicated.

$$(1-C_{V_{CHIN}}) = (1-C_{V_{COMP}}) \times 1.3$$

$$C_{V_{CHIN}} = (1-C_{V_{COMP}})1.3-1$$

This analysis predicts a chin nozzle C_V 1% below the composite C_V at 48/52 split, and 4% below for the 71/29 split without spacers. These values reflect low fan total pressure in the lower sector exhausting through the chin nozzle, duct losses due to the internal friction and flow across the centerbody and chin nozzle cascade losses.

The accuracy of above approximations depends on the true thrust direction of the nozzles, and particularly that of the chin nozzle for the 71/29 split. The error in $C_{V_{COMP}}$ for a 5^0 deviation from the assumed 75^0 thrust direction is derived below:

$$\frac{\Delta C_{V_{COMP}}}{C_{V_{COMP}}} = \frac{\frac{F_{NORM}\left(\frac{1}{\sin 75^0} - \frac{1}{\sin 70^0}\right) + F_{NORM}\ (\text{ctg } 70^0 - \text{ctg } 75^0)}{W_{FAN/g}\ V_{IDEAL,FAN}}}{\frac{F_{NORM}\ \frac{1}{\sin 75^0} + \frac{F_{AXIAL}}{F_{NORM}} - F_{NORM}\ \text{ctg } 75^0}{W_{FAN/g}\ V_{IDEAL}}}$$

= .04 for the 71/29 split with cambered blades

Evaluation of oil flow photographs such as Fig. 12 reveal that most of the flow exits at 70^0 to 80^0, suggesting that the error contribution of the actual thrust angle to $C_{V_{COMP}}$ is less than 4%. Oil flow photographs were not produced for the case of flat blade cascade, which could have a different thrust angle. A steeper discharge angle would explain a lower $C_{V_{COMP}}$ for this case.

Repeatability of the data is illustrated on Fig. 16. Data were generally taken from 60% RPM to 90% in 5% increments, then down to 60% in 10% increments. In addition, Run 21 was a repeat of Run 14. The data show that most points within one run fall within a 2% band, and that the shift between runs was also about 2%. Therefore, differences among test configurations in excess of about 3% can be considered significant.

Effect of Flow Split

The effect of flow split on the fan discharge total pressure distribution is shown on Figs. 17-18. Rake total pressure profiles are shown on Fig. 17 and ring profiles on Fig. 18. The chin nozzle was discharging in the

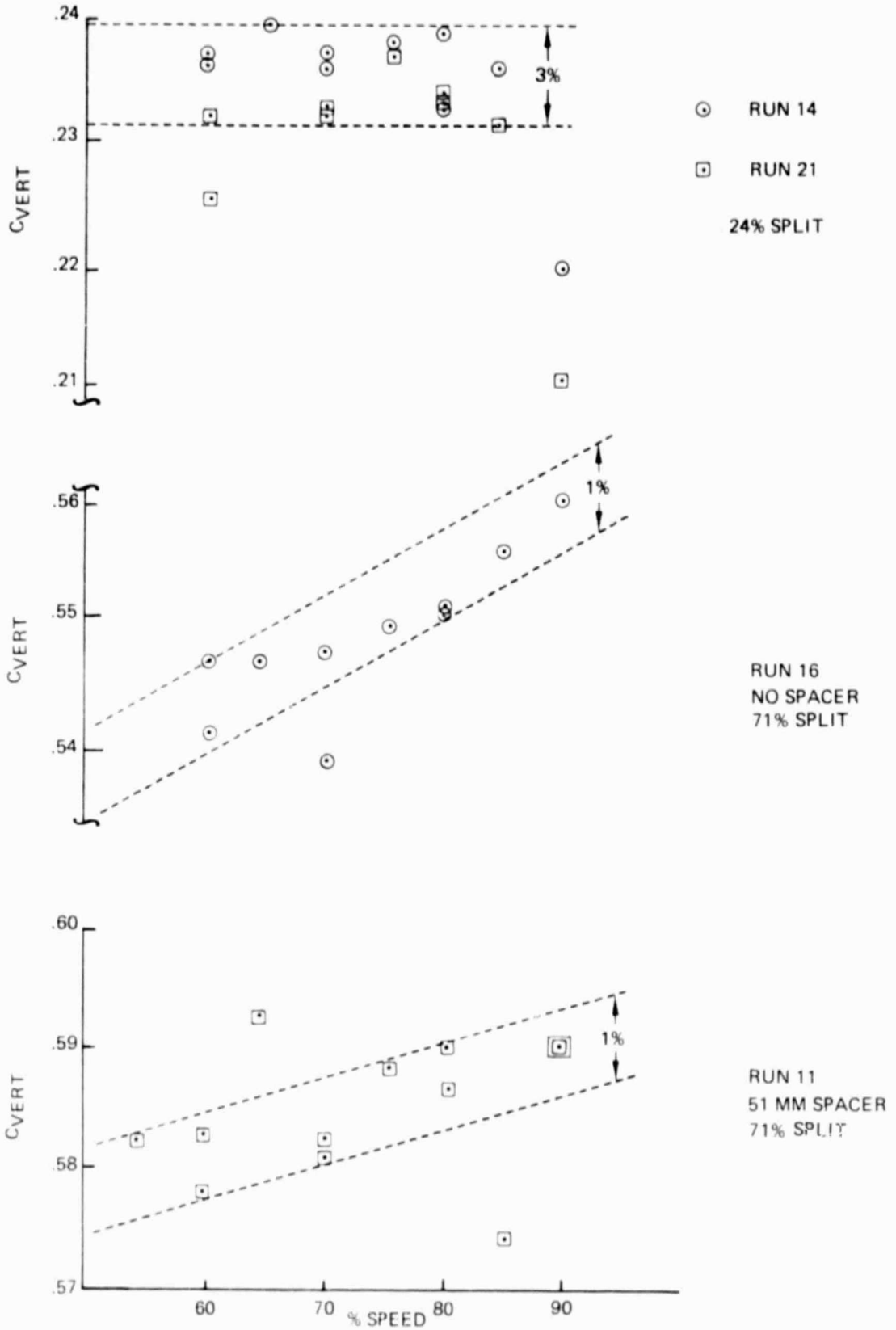

Figure 16. Repeatability of Vertical Thrust Coefficient

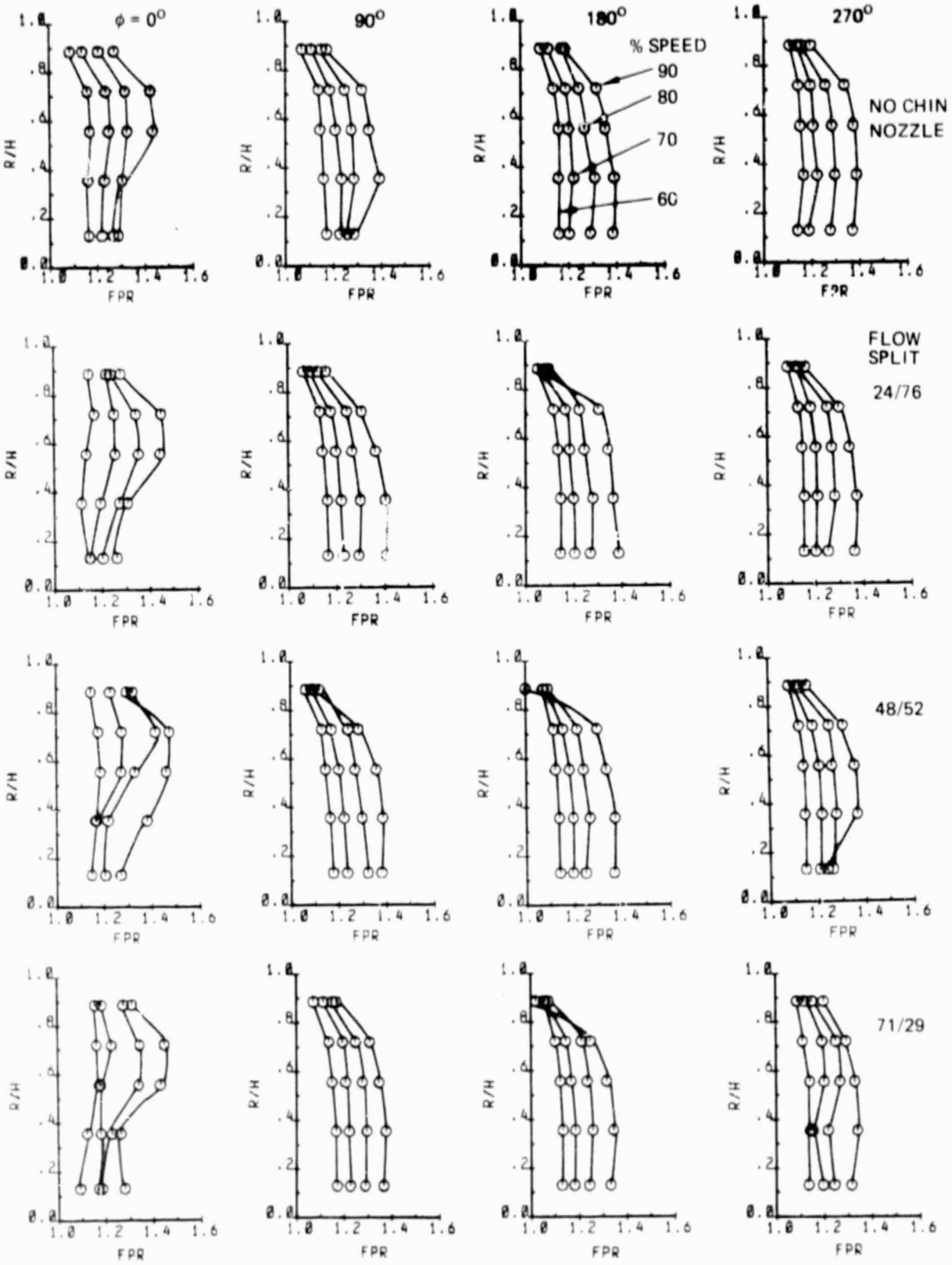

Figure 17. Effect of Flow Split on Rake Total Pressure Profiles No Spacer

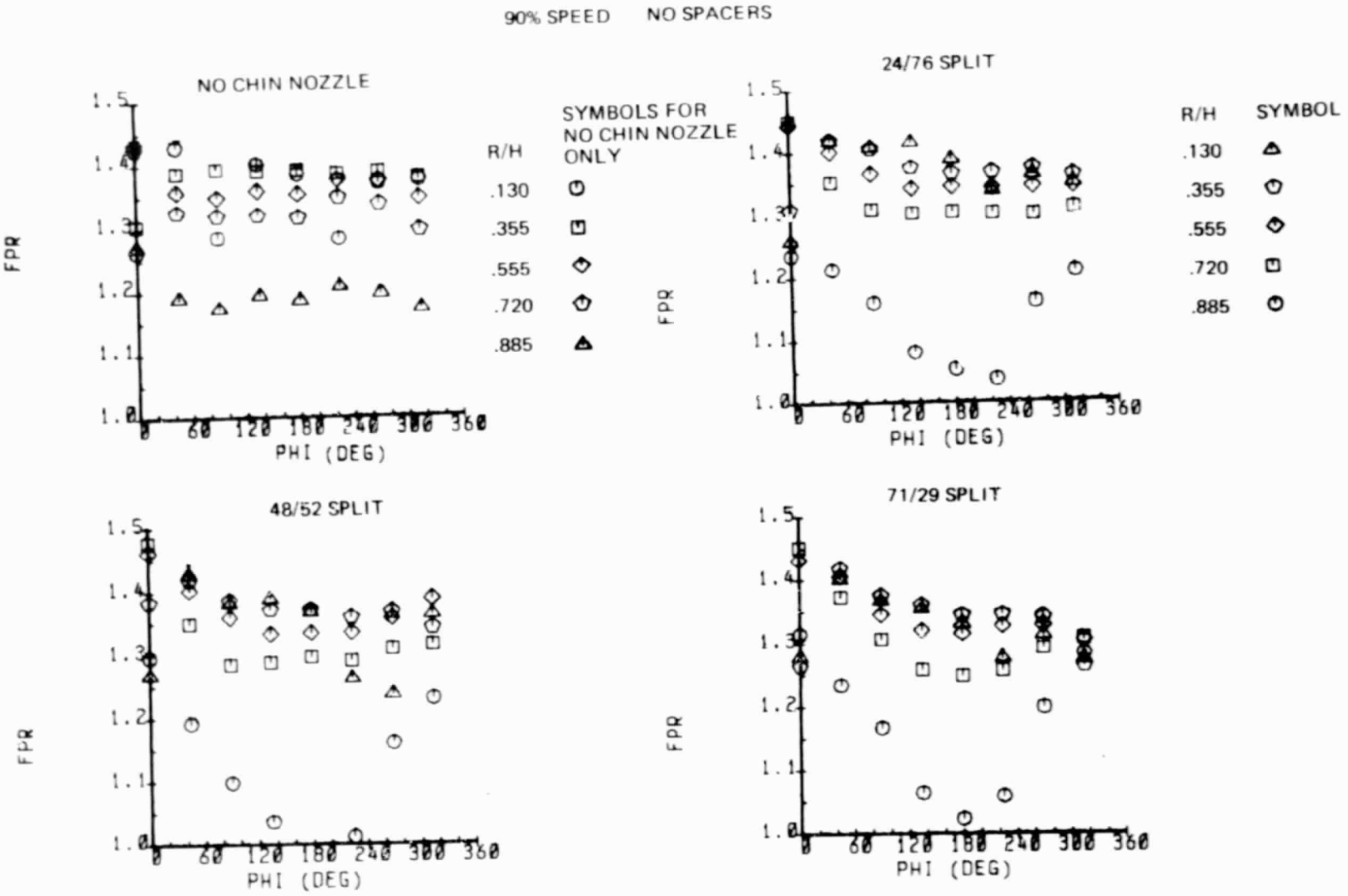

Figure 18. Effect of Flow Split on Peripheral Rake Distortion

direction of ϕ (PHI) = 180°. It is seen that the greatest disturbance occurs at the 48/52% flow split, with the fan work at the tip decreasing at 180° and increasing at 0°. Static pressure readings behind the fan on the cowl and centerbody, Fig. 19, are similar for 48/52 and 71/29 flow splits, indicating that the local geometry is more important than the flow split. Fig. 20 shows pressure data down the cowl and centerbody at the maximum flow through the chin nozzle. Location 1 on the cowl and location 2 on the centerbody show the greatest nonuniformity. While the low pressure at 180° on the cowl is caused by the local wall curvature, the low pressure on the centerbody at location 2 at 180° is probably due to a vortex in that area, as indicated by flow visualization results on Fig. 11.

Effect of Spacer Length

Spacer length has a noticeable effect on the fan. Fig. 21 compares fan total pressure distributions with the chin nozzle vs spacer length and with the conventional, axisymmetric duct and nozzle. It is seen that the peripheral total pressure distortion decreases as the spacer length is increased. Static pressure distortion immediately behind the fan is also decreased with increasing spacing, see Fig. 22. The static pressure distortion on the cowl, however, is increased as spacer length is increased. This is illustrated on Fig. 22. This distortion is primarily a function of local wall curvature and Mach number. It increases with the spacing because the effect of the fan total pressure defect in the lower segment is progressively washed out by mixing as the distance to the chin nozzle increases.

Effect of Chin Nozzle Closing Schedule

Flow and thrust transfer from the chin nozzle towards the aft nozzle for pitch control or transition can be accomplished by progressively closing passages between vanes starting with the front passage, with the aft passage, or simultaneously from both ends. The open area at reduced flow rates can therefore be shifted fore and aft. Tests at all three positions showed virtually no effect on the fan total pressure distribution, as seen in Fig. 23. The effect on statics and vertical thrust was also insignificant.

Effect of Vane Removal

Thrust measurements have shown that the effectiveness of the wide-open chin nozzle is well below design values, and flow visualization indicated separation on the aft vanes. Tests with the aft vane removed showed no improvement in vertical thrust fraction. There was also little effect on the fan discharge pressure distortion, as illustrated in Fig. 24. Removing the aft vane had virtually no effect, while removing all vanes had a slight effect in the tip region of the fan over the lower quadrant, next to the chin nozzle. Removal of all vanes reduced C_{VERT} due to a decrease in chin nozzle discharge angle.

Performance With Flat Vane Cascade

Flow visualization results indicated that considerable turning is accomplished within the cowl approaching the chin nozzle cascade, and that the

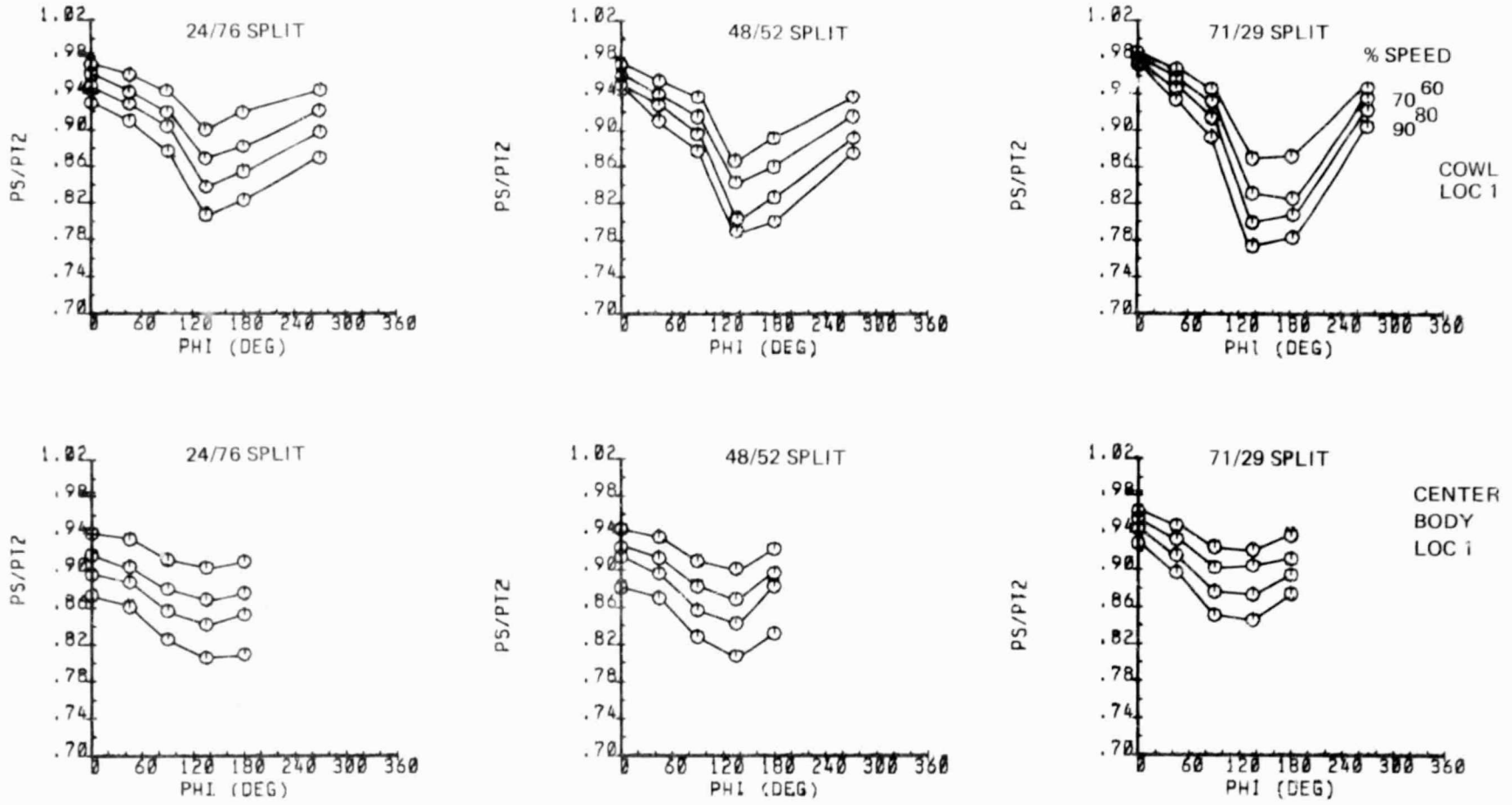

Figure 19. Effect of Flow Split on Peripheral Static Pressure Distortion on Cowl and Centerbody

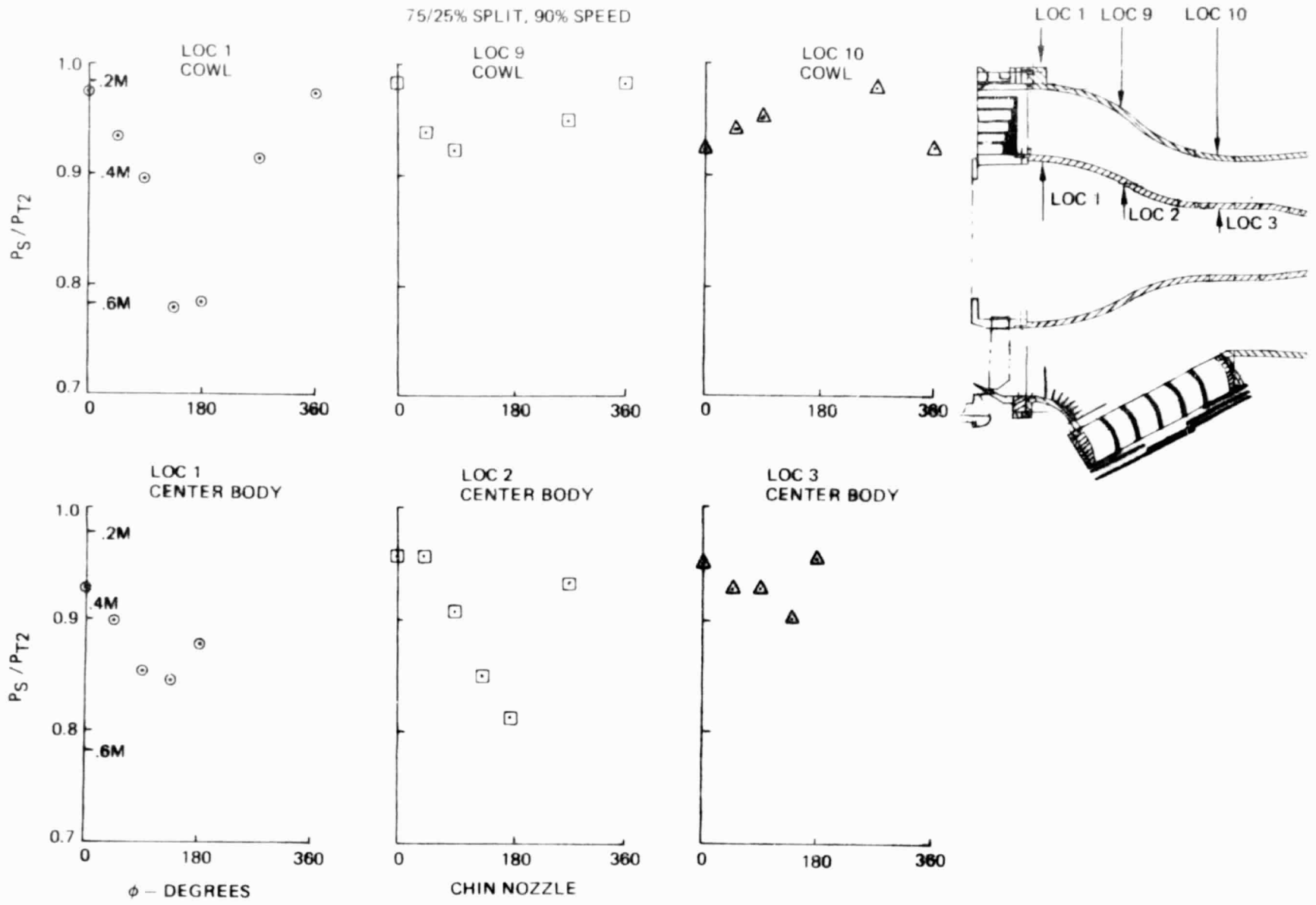

Figure 20. Cowl and Centerbody Peripheral Pressure Distribution

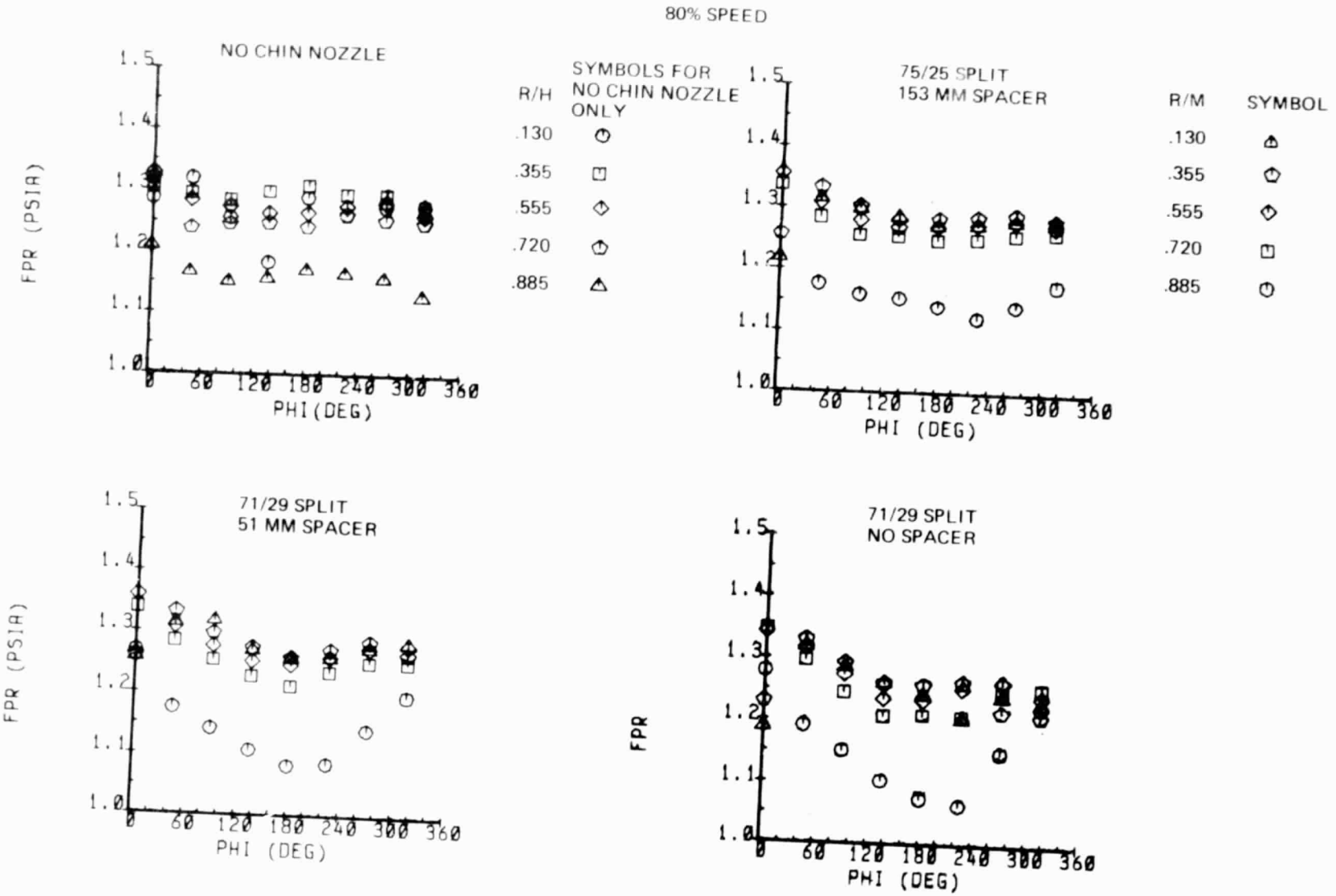

Figure 21. Effect of Spacers on Peripheral Rake Distortion

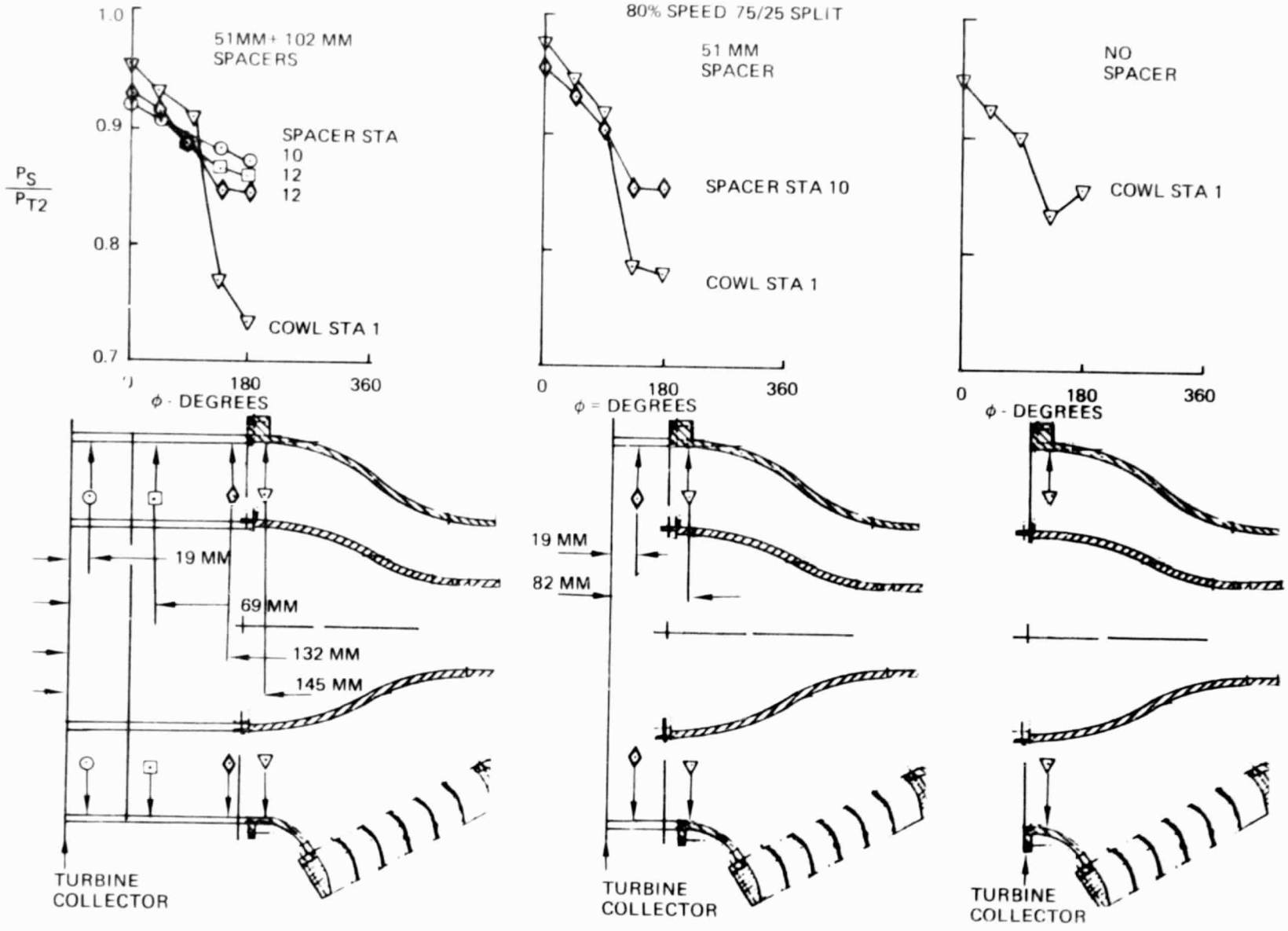

Figure 22. Effect of Spacers on Static Pressure Distributions

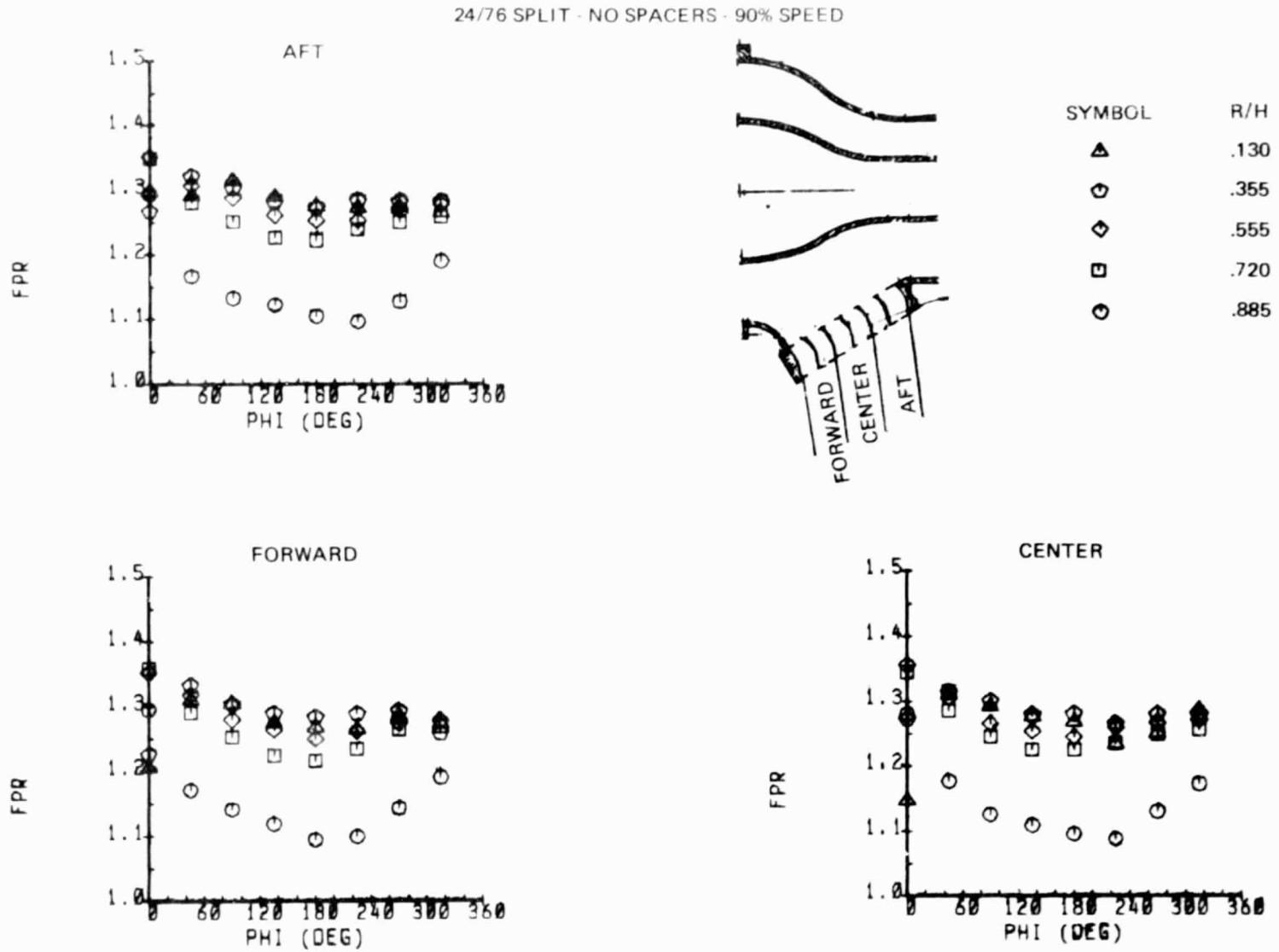

Figure 23. Effect of Position of Chin Nozzle Opening

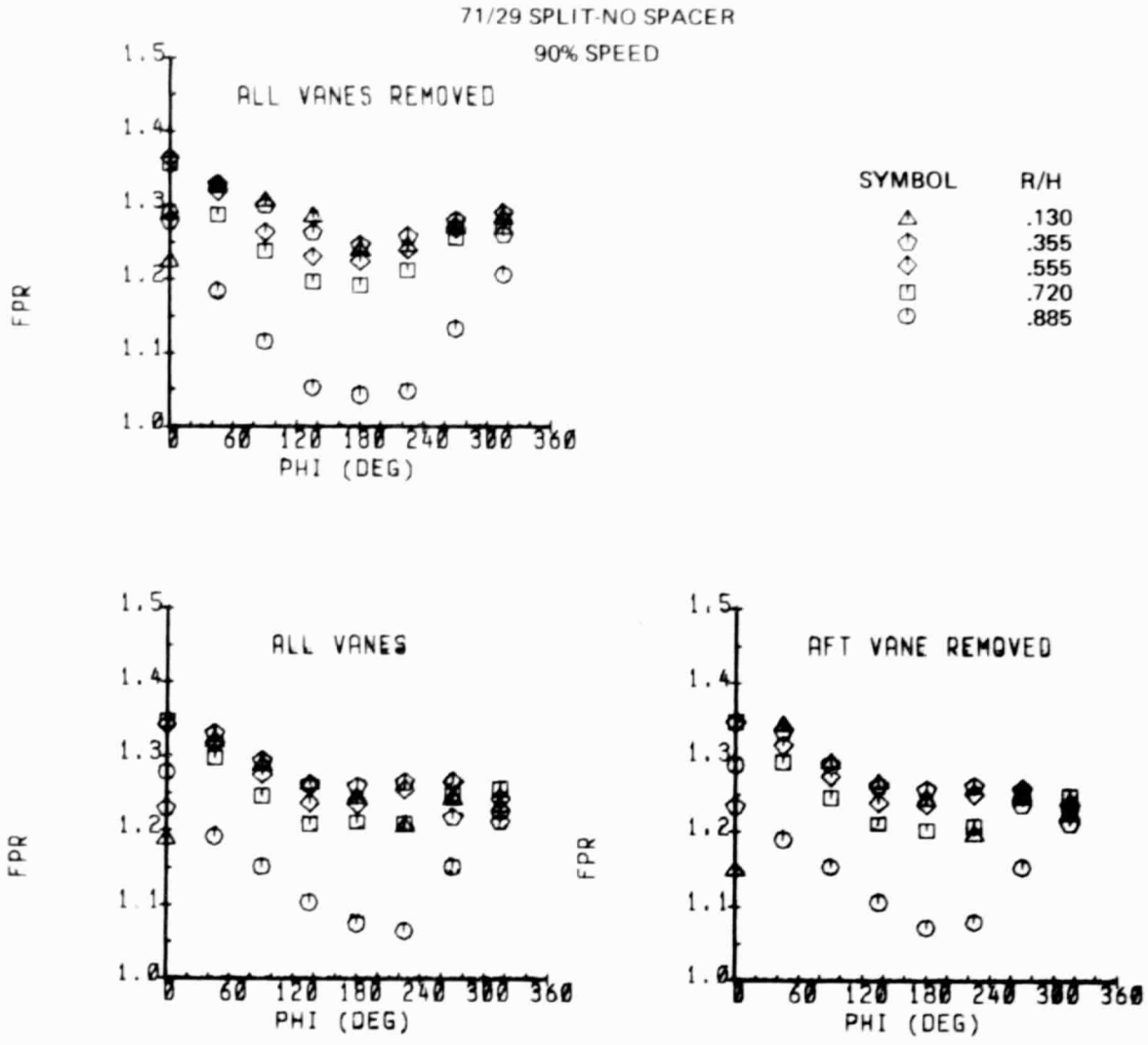

Figure 24. Effect of Vane Removal on Ring Pressures

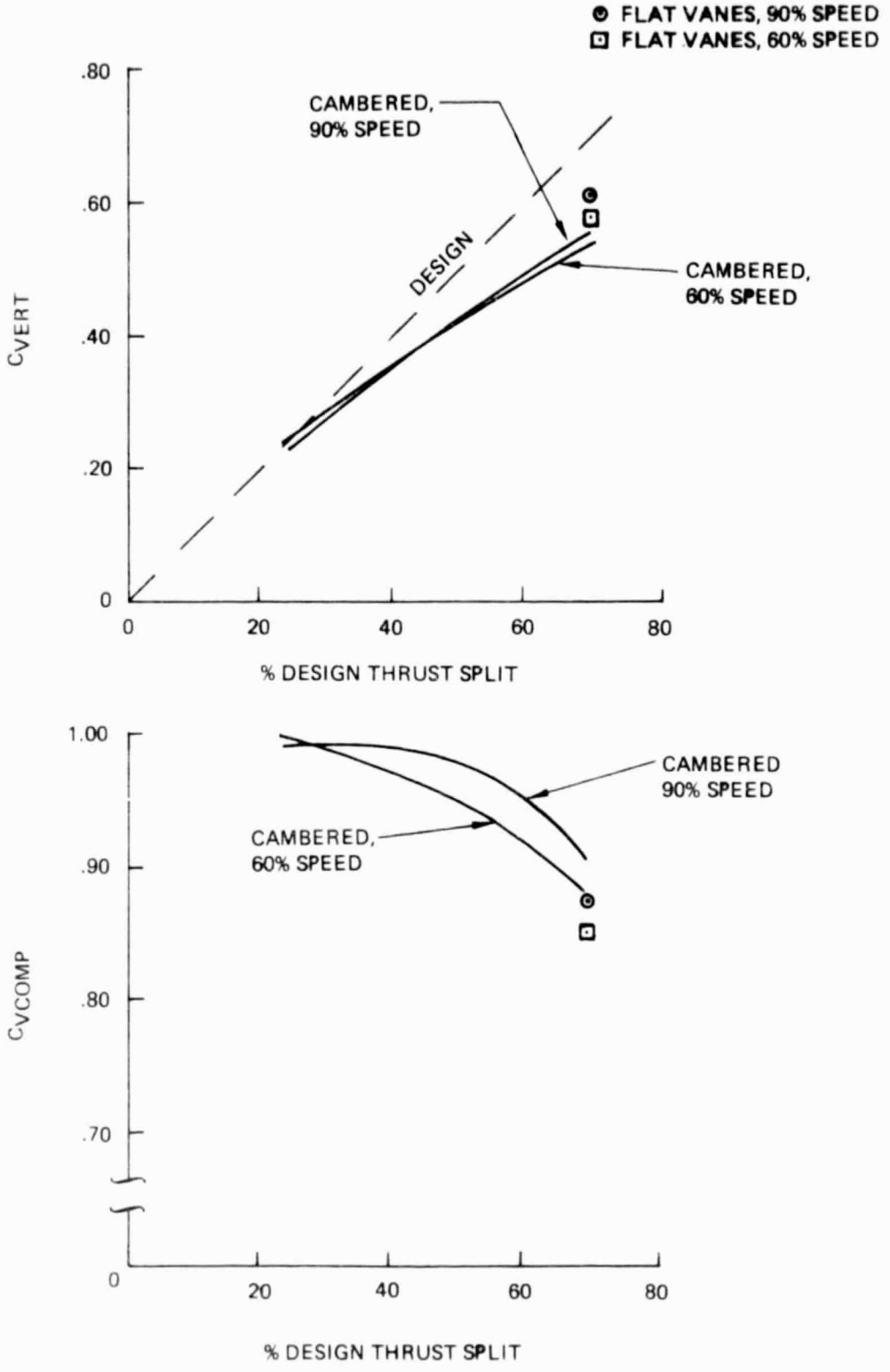

Figure 25. Thrust Performance of Flat-Vane Cascade

leading edge angle of the aft blades in particular was too low, resulting in a negative angle-of-attack. A set of flat vanes was installed in the cascade frame at 75° to the horizontal. One force and pressure data run was obtained on this set before it failed. The results are shown on Figure 25. The vertical thrust coefficient improved 10% and the composite velocity coefficient decreased relative to the cambered cascade. This result suggests that the discharge angle of the flat-vane cascade was steeper. No flow visualization was obtained due to the failure of the blades. A decrease of the measured axial force also suggests a steeper discharge angle for the flat-vane chin nozzle.

CONCLUSIONS

Operation of the chin nozzle in proximity to the fan discharge produced a localized drop in fan total pressure ratio in the tip region over the quadrant nearest the chin nozzle. The disturbance was caused primarily by the local cowl wall curvature. Varying the flow through the chin nozzle had little effect on the disturbance.

The chin nozzle was quite effective as a thrust deflection device at thrust splits up to 50/50% front/aft. At the highest design front thrust tested, 71 to 75% of the total thrust, the measured front thrust was 55 to 65%. Lack of accurate flow and thrust calibrations (planned for a second test) prevented further analysis of the chin nozzle performance. At this time, it is not known whether the lack of vertical thrust is due to a low flow coefficient (effective area), or low velocity coefficient (pressure losses) in the chin nozzle, internal pressure losses, vortices and secondary flows due to flow across the centerbody, or excessive spreading of the exit flow (cancellation of thrust vector components). Oil flow visualization showed that much of the cascade was separated on the pressure (concave) side and that the flow approaching the cascade contained strong vortices.

Oil flow visualization also showed a crossflow in the area where the core engine inlets would be located. This problem must be addressed in the core inlet design to prevent core engine stalls.

LIST OF REFERENCES

1. Deflector/Nozzle Program, Contract N00019-72-C-0612, Final Report, PWA4910